Peña González, C.E., García Broncado, P., Ottaviani , M.F., Cangiotti , M., Fattori , A., Hierro Oliva, M., González Martín, M.L., Pérez Serrano, J., Gómez Ramírez, R., Muñoz Fernández, M.Á., Sánchez-Nieves Fernández, J. & Mata De La Mata, Francisco J. De La 2016, "Dendronized Anionic Gold Nanoparticles: Synthesis, Characterization and Antiviral Activity", Chemistry - A European Journal, vol. 22, no. 9, pp. 2987-2999.

Available at http://dx.doi.org/10.1002/chem.201504262

Dendronized Anionic Gold Nanoparticles: Synthesis, Characterization and Antiviral Activity

Cornelia E. Peña-González,[a] Pilar García-Broncano,[b,c] M. Francesca Ottaviani,[d] Michela Cangiotti,[d] Alberto Fattori,[d] Margarita Hierro-Oliva,[e,f] M. Luisa González-Martín,[e,f] Jorge Pérez-Serrano,[g] Rafael Gómez,[a,f] M. Ángeles Muñoz-Fernández,[c,f] Javier Sánchez-Nieves,[a,f,] F. Javier de la Mata[a,f,*]*

[a] Cornelia E. Peña-González, Dr. Rafael Gómez, Dr. Javier Sánchez-Nieves, Dr. F. Javier de la Mata.

Dpto. de Química Orgánica y Química Inorgánica, Campus Universitario, Universidad de Alcalá, Alcalá de Henares (Madrid) Spain; e-mail javier.delamata@uah.es, javier.sancheznieves@uah.es.

[b] Pilar García-Broncano.

Unidad de Infección Viral e Inmunidad, Centro Nacional de Microbiología, Instituto de Salud Carlos III (Campus Majadahonda), Madrid, Spain.

[c] Pilar García-Broncano, Prof. M. Ángeles Muñoz-Fernández.

Laboratorio de InmunoBiología Molecular. Hospital General Universitario Gregorio Marañón, Madrid, Spain. Instituto de Investigación Sanitaria Gregorio Marañón, Madrid, Spain; Spanish HIV HGM BioBank, Madrid, Spain.

[d] Prof. M. Francesca Ottaviani, Dr. Michela Cangiotti, Dr. Alberto Fattori.

Department of Earth, Life and Environment Sciences, University of Urbino, Urbino, 61029 Italy.

[e] Margarita Hierro-Oliva, Prof. M. Luisa González-Martín.

Departamento de Física Aplicada, Facultad de Ciencias, Campus Universitario, Universidad de Extremadura, Badajoz (Spain).

[f] Dr. Rafael Gómez, Dr. Javier Sánchez-Nieves, Dr. F. Javier de la Mata, Prof. M. Ángeles Muñoz-Fernández, Margarita Hierro-Oliva, Prof. M. Luisa González-Martín.

Networking Research Center for Bioengineering, Biomaterials and Nanomedicine (CIBER-BBN).

[g] Dr. Jorge Pérez-Serrano

Departamento de Biomedicina y Biotecnología, Universidad de Alcalá, Campus Universitario, E-28871, Alcalá de Henares, Spain.

Abstract

Anionic carbosilane dendrons decorated with sulfonate functions and with a thiol moiety at the focal point have been used to synthesize water soluble gold nanoparticles (AuNPs) by direct reaction of dendrons, gold precursor and reducing agent in water and also by place-exchange reaction. These nanoparticles have been characterized by nuclear magnetic resonance (NMR), transmission electron microscopy (TEM), thermogravimetric analysis (TGA), X-ray photoelectron spectroscopy (XPS), UV, elemental analysis, and Z potential. Also, the interacting ability of the anionic sulfonate functions was investigated by electron paramagnetic resonance (EPR) using copper(II) as a probe. It was found that the different structures and conformations of the AuNPs modulate the availability of sulfonate and thiol groups to be complexed by copper(II). Toxicity assays of AuNPs showed that those produced by direct reaction were less toxic than those obtained by ligand exchange. Inhibition of HIV-1 infection was higher for dendronized AuNPs than for dendrons.

1. Introduction

The properties of nanoparticles, especially metal nanoparticles,[1] such as large surface-to-volume ratio, stability, excellent biocompatibility, low toxicity,[2] and the ease to functionalize make them very attractive for biomedical applications.[3-5] Among them, gold nanoparticles (AuNP) are being extensively explored by their inertness and lesser cytotoxicity.[6] A potential application of these systems is as multivalent drug, leading to an important increase of activity with respect to monovalent compounds presenting the same functional group.[7, 8] Under this premise, several AuNPs have been developed to fight against one of the most important pandemic, AIDS, caused by human immunodeficiency virus type 1 (HIV-1). It is due to the fact that there is no vaccine against HIV-1 and therefore, the research in microbicides has grown considerably.[9]

TAK-779 is an antagonist of CCR5, which is a co-receptor for HIV-1 strains, but with poor pharmacologic properties due to the presence of an ammonium group in its structure. SDC-1721 is a modification of TAK-779 with low affinity to this receptor and biological inactive, but without the positive charge. However, the coating of AuNPs with SDC-1721 created a system with high inhibition of HIV-1 fusion.[10] On the other hand, the HIV-1 glycoprotein gp120 is highly glycosylated with high-mannose type glycans arranged in clusters. Mimicking this arrangement, multivalent oligomannoside platforms as AuNPs have been developed to create antivirals, showing inhibition of HIV-1 infection in human cells.[11, 12] Moreover, polyanionic AuNPs decorated with long linear chains with sulfate groups are active against the X4 tropic NL4.3 Renilla HIV-1 recombinant virus in infected MT-2 cells by blocking viral receptors.[13] Also, other anionic AuNPs with polyglycolsulfate dendrons efficiently inhibit the binding of vesicular stomatitis virus (VSV) to cells.[14] With respect to the inhibition of HIV-1 infection, the antiviral activity of polyanionic compounds is well known.[15-18] Their mechanism is associated with electrostatic interactions between the HIV envelope protein gp120 and the anionic moieties of these agents that ultimately prevent binding of the virus to the target cells.[15] Hence, they would act as entry inhibitors. This mode of action would favor its formulation as microbicide gel. However, also has been reported the

interactions with cell surface markers like CD4, CXCR4 or CCR5 or the triggering of a series of events that inhibit some steps of viral replication.[19, 20]

Dendrimers are macromolecules with well-defined size and structure, monodisperse and with a multivalent molecular surface.[21-26] As for AuNPs, these characteristics make them very attractive for biomedical applications and anionic dendrimers are being explored as anti-HIV agents.[22, 27-30]. We work on dendritic carbosilane molecules and we have developed anionic dendrimers that efficiently inhibit HIV-1 infection.[19, 31-33] The type of dendrimer core and of anionic function affect slightly their affinities toward gp120 or cell receptors. Moreover, a combination of several dendrimers showed synergistic effects.[34, 35] Of the library of compounds studied, those presenting sulfonate groups demonstrated great potency to be formulated as a microbicide gel (named as 2G-SF16).[19] However, one disadvantage of dendrimers is the usual high number of synthetic steps to obtain them, notably if high generation derivatives are required. This drawback is remarkable in compound 2G-SF16 and other synthetic strategies have been employed to ease the preparation of anionic systems, as thiol-ene addition.[36] The compounds thus obtained showed also important anti-HIV properties.[35] Furthermore, the thiol-ene approach proved its value in the synthesis of dendrons.[36]

Dendrons are molecules similar to dendrimers with analogous properties, but instead of presenting spherical shape they are cone-shaped with two different functions, the focal point and the dendron surface. Whereas the dendron surface has the same functional design like dendrimers, the focal point can be used as an anchor,[37] for modifying properties of polymers,[38] for stabilizing nanoparticles,[39-43] for improving biological activity of functional molecules,[44-47] and for other purposes.[48, 49] Therefore, an advantage of dendrons over dendrimers is the possibility to translate the multivalency to nanoscopic systems,[37] a process known as dendronization. This process has the advantage of reducing costs because it is not required the synthesis of high generation systems. Recently, we have developed a synthetic platform of carbosilane dendrons[36, 50] that have provoked the surface modification of poly(D,L-lactide-co-glycolide) acid nanoparticles[51] and mesoporous nanoparticles[52] for nucleic acid delivery, labelling them with a dye,[36, 53] or acting as drug carrier in antibacterial compounds.[54] In the case of NPs, the antiviral activity

or RNA transfecting efficacy was improved by dendronization of these systems, whereas dendrons by themselves are not able to exert the same behavior. Regarding metal NPs, only one example in the scientific literature reports about such systems covered with carbosilane dendrons.[55]

The relevance of both AuNPs and anionic dendrimers in the search of alternative therapies against HIV-1 has triggered our efforts to obtain new multivalent anionic nanosystems with the aim to combine their benefits. With this in mind, herein we report the synthesis of carbosilane dendrons decorated with peripheral sulfonate moieties and a thiol function at the focal point that have been employed to stabilize AuNPs. The sulfonate groups are responsible for the anionic charge and also favor the solubility in water. These AuNPs-containing dendrons were characterized by nuclear magnetic resonance (NMR), transmission electron microscopy (TEM), thermogravimetric analysis (TGA), X-ray photoelectron spectroscopy (XPS), UV, elemental analysis, and Z potential. Also, we have used Cu^{II} cations as spin probes to analyze the interacting ability of the anionic sulfonate functions by electron paramagnetic resonance (EPR) spectroscopy. The toxicity and antiviral properties against HIV of the anionic dendrons and NPs thus prepared have been evaluated.

2. Results and Discussion

2.1 Synthesis of dendrons

Previously to the synthesis of anionic AuNP it was needed to develop dendrons adequately functionalized to trap AuNPs and also to support the anionic charge. The first function is achieved by the presence of a thiol moiety at the focal point, due to the affinity of gold toward sulfur containing ligands. The second one is obtained by the introduction of sulfonate groups at the periphery. The starting compounds were dendrons with a thioacetate moiety at the focal point, precursor of thiol groups, and peripheral vinyl functions, $(MeCOS)G_nV_m$ (n = 1, m = 2; n = 2, m = 4; n = 3, m = 8).[50] The vinyl functions are suitable to introduce the desired sulfonate anions by thiol-ene addition,[36] whereas the thioacetate focal point can be transformed under soft conditions into a thiol moiety. For simplicity, the dendrons are named in this work as $XG_n(Y)_m$, where X indicates the nature of the focal point, G_n the

dendron generation and $(Y)_m$ the peripheral function and its number (V for vinyl and SO_3^- for the sulfonate groups, see Scheme 1).

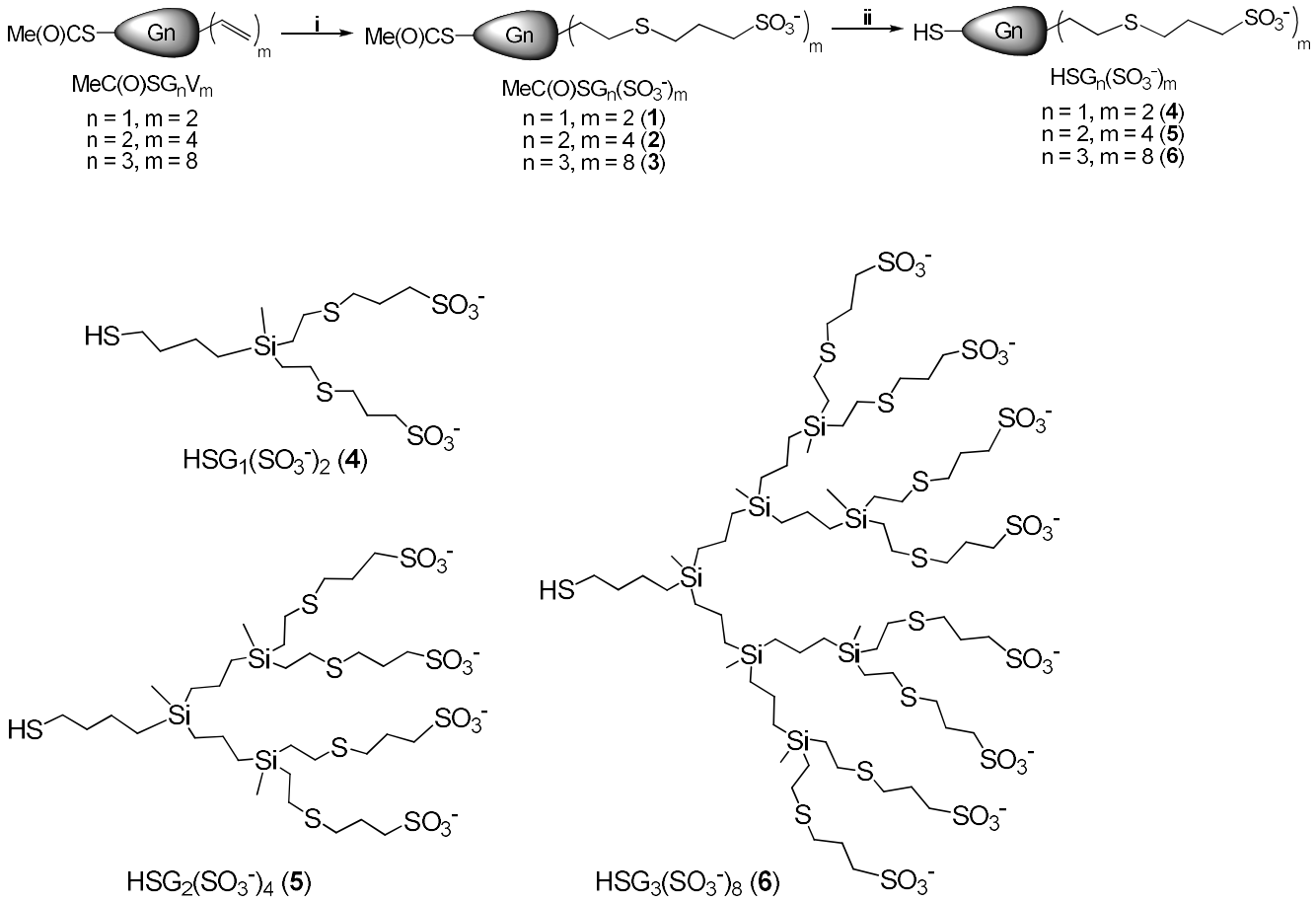

Scheme 1. Top: Synthesis of anionic dendrons $HSG_n(SO_3^-)_m$ (n = 1, m = 2 (**4**); n = 2, m = 4 (**5**); n = 3, m = 8 (**6**)). i) $HS(CH_2)_3SO_3^-$, DMPA, hν; ii) HCl. Bottom: Sturctures of dendrons $HSG_n(SO_3^-)_m$ (**4**-**6**).

Hence, the reaction of $(MeCOS)G_nV_m$ (n = 1, m = 2; n = 2, m = 4; n = 3, m = 8)[50] with sodium 3-mercapto-1-propanesulfonate ($HS(CH_2)_3SO_3Na$) under UV irradiation enabled us to obtain the anionic compounds $(MeCOS)G_n(SO_3^-)_m$ (n = 1, m = 2 (**1**); n = 2, m = 4 (**2**); n = 3, m = 8 (**3**)) as white solids (Scheme 1), which where water soluble. ^{1}H-NMR spectroscopy showed the disappearance of the vinyl functions and formation of the chain $Si(CH_2)_2S$ from the thiol-ene addition. Also, the resonances of the chain $S(CH_2)_3SO_3$ were observed as three multiplets between 1.9 and 3.0 ppm. These two fragments were clearly identified in the ^{13}C-NMR spectra. The ^{1}H-^{29}Si HMBC spectra clearly detected the shifting of the resonance of the outermost Si atom from ca. δ -14.0 in $(MeCOS)G_nV_m$ to ca. δ 2.5 in **1**-**3**. Continuously,

deprotection of the focal point was achieved by heating with HCl in MeOH, giving $HSG_n(SO_3^-)_m$ (n = 1, m = 2 (**4**); n = 2, m = 4 (**5**); n = 3, m = 8 (**6**); Scheme 1). Again, the ^{1}H-NMR spectra were helpful to determine this transformation. The Me group of the precursor focal point is not observed and the proton resonance of the methylene $HSCH_2$ shifted from ca. δ 2.82 to ca. δ 2.55. However, the acid HS proton resonance could not be detected in D_2O. In ^{13}C-NMR spectroscopy, the chemical shift of this methylene belonging to the focal point $HSCH_2$ shifted from ca. δ 28.4 in compounds **1-3** to ca. δ 22.2 in compounds **4-6**. Finally, the carbonyl present in the starting compounds was not observed. The disappearance of this function was also detected by IR.

2.2 Synthesis of gold nanoparticles (AuNP)

As commented above, we are interested in biomedical applications of anionic nanoparticles containing sulfonate dendrons **4-6**, with two, four and eight groups. To properly compared the influence of these anionic dendrons in synthesis and activity of AuNPs, we considered that preparation of AuNPs decorated with monosulfonate ligands was also necessary. With this in mind, we have also used compound $HS(CH_2)_3SO_3^-$ as capping ligand for AuNPs preparation. For the synthesis of gold nanoparticles we have employed two different approaches: Brust-Schriffin method (direct method) and place-exchange reaction.

The Brust and Schriffin method implies the reduction of gold precursor in the presence of a stabilizing agent for the NPs, which in our case will be dendrons **4-6**. The final size of the AuNPs depends on factors as Au/ligand relationship, amount of reducing agent, reaction time. Initially, we chose a Au:dendron proportion 1:1. We carried out the reaction by adding dropwise a water solution of dendrons **4-6** to a water solution of $[AuCl_4]^-$, followed by further dropwise addition of a water solution of $NaBH_4$, stirring the reaction mixture for several hours and finally dialysis of the solution (MWCO 10 KDa). However, with this ratio only AuNPs were formed from dendron **4** (Au@($SG_1(SO_3^-)_2$), **7a**) (Scheme 2). The AuNPs thus prepared were of 2.4 nm of diameter (measured by TEM) and water soluble.

We have to consider that gold has high affinity for sulfur, and these dendrons contain other S atoms in their scaffold apart from that of the focal point. Additionally, the anionic system $S(CH_2)_3SO_3^-$ can act as

chelating agent.[56, 57] Thus, to minimize the trapping ability of these outer groups we diminished the Au:dendron ratio in the reaction, using as reference the number of sulfonate groups of the wedge. Hence, the new Au:dendron relations for the reaction were 2:1 for **4**, 4:1 for **5**, and 8:1 for **6**. With these considerations, the same procedure described above was successful, rendering water soluble gold nanoparticles for the three dendrons (scheme 2, Au@($SG_n(SO_3^-)_m$); n = 1, m = 2 (**7b**); n = 2, m = 4 (**8b**); n = 3, m = 8 (**9b**)). Compounds **7b-9b** were characterized by TEM, TGA, elemental analysis, XPS, ^1H NMR, UV and Z potential (Table 1), and resulted to be very stable (> 18 months). When this protocol was applied to the monosulfonate ligand $HS(CH_2)_3SO_3^-$ (Au:S ratio 1:1) very low yield of NPs were obtained. Moreover, these NPs aggregated within few days (see Supporting Information).

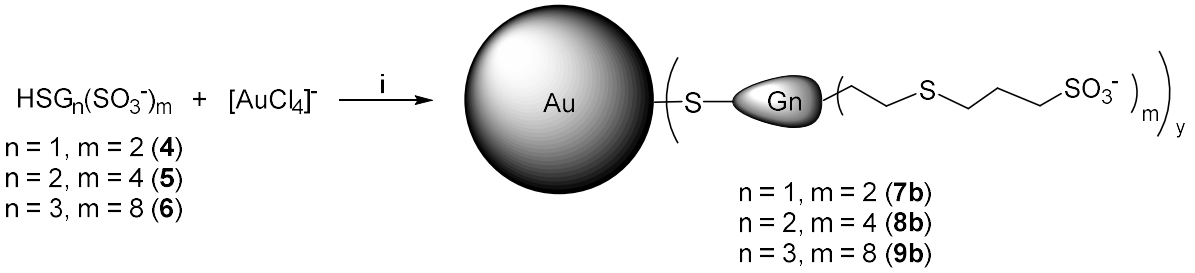

Scheme 2. Synthesis of anionic NPs Au@($SG_n(SO_3^-)_m$) (n = 1, m = 2 (**7b**); n = 2, m = 4 (**8b**); n = 3, m = 8 (**9b**)). i) $NaBH_4$.

Table 1 collects a survey of physical and chemical properties of AuNPs. TEM images showed formation of these AuNP with sizes ranging from 3.0 to 3.6 nm (Figures 1 and Supporting Information). These sizes belong to the gold core, as dendrons don't have enough contrast to be detected. Reduction of dendron proportion for the synthesis of AuNPs derived from **4**, **7a** and **7b**, has as consequence an increase in the size. In contrast, the reduction of the amount of dendron as explained above for formation of AuNPs **7b-9b**, led to a slightly decrease of the size. As expected, minor sizes correspond to less dendrons on the surface, calculated from TGA and TEM data, and consequently less sulfonate moieties on the surface are observed (510 for **7b**, 484 for **8b**, 328 for **9b**). However, the proportion between the number of gold atoms and sulfonate anions is similar for the three AuNPs (2.8 for **7b** and 2.5 for **8b** and **9b**), indicating a similar

effectiveness of AuNPs formation with these Au/dendron ratios. The combination of data obtained from TGA and elemental analysis allowed the calculation of average MW for these systems.

As consequence of the AuNPs **7-9** sizes, we could expect a favorable biocompatibility of our systems. Several studies reflects the relationship between toxicity and size, in general being smaller systems clearly more biocompatible.[58] This is particular relevant when the capping groups are anionic, due to the higher tolerance provided by these type of functions.[59] One of the reasons of lower toxicity for smaller systems is that systems with diameters below 6 nm can be cleared from the body by renal execration, which would diminish problems associated with accumulation.[60, 61]

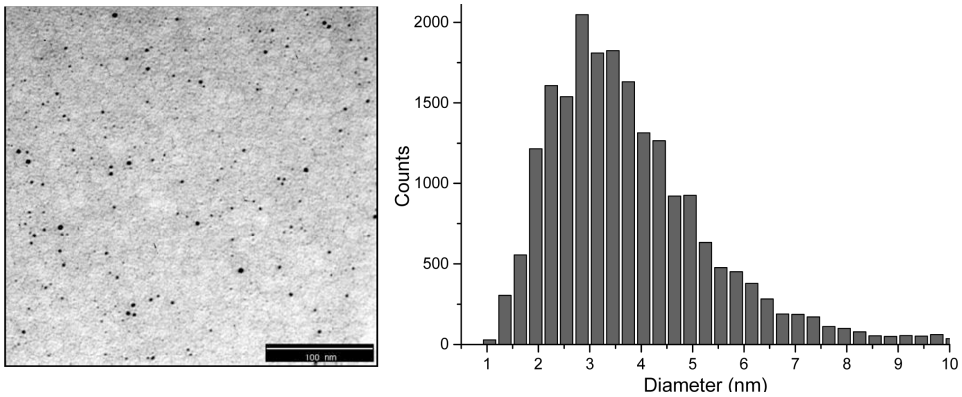

Figure 1. **Au@(SG1(SO$_3$Na)$_2$) (7b)**: a) TEM image and, b) Size distribution histogram associated to nanoparticle **7b** functionalized by direct method with sulfonate carbosilane dendrons of first generation (average size = 3.6 nm (20668 measure nanoparticles with Image J program)).

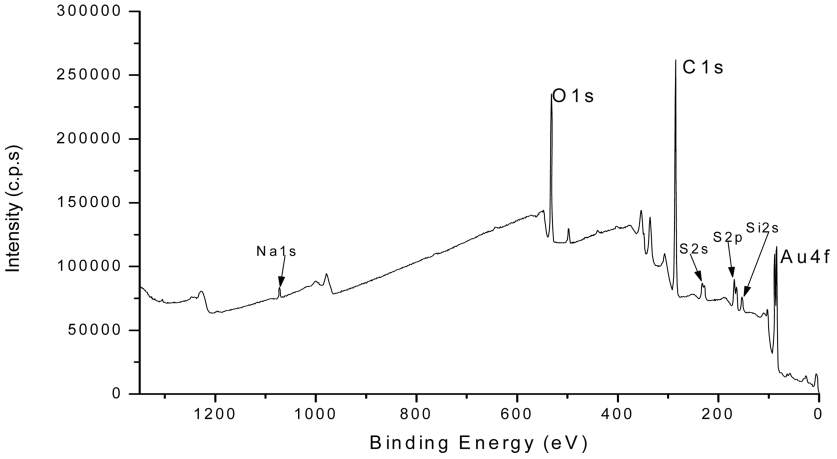

Figure 2. XPS survey spectrum collected for Au@(SG1(SO$_3$Na)$_2$) (**7b**), as a representative example of all the samples examined.

XPS was relevant to determine the presence of the chemical functional groups that belong to the NP. As a representative example, the XPS survey spectrum collected for Au@(SG1($SO_3Na)_2$) (**7b**) is shown in Figure 2. Survey spectra for other samples can be found in Supplementary Materials. Also high resolution spectra for different regions were collected to analyze the bonding interaction between the different elements. Figure 3 includes the S2p region of the spectra. Two peaks appear clearly when deconvolution is applied to the spectra. One of them, associated to S atoms bound to Au, is placed at 163.2 eV, 163.5 eV and 163.4 eV, for Au@(SG1($SO_3Na)_2$) (**7b**), Au@($SG_2(SO_3Na)_4$) (**8b**), and Au@($SG_3(SO_3Na)_8$) (**9b**) conjugates, respectively. The other peak, at 168.3 eV, 168.4 eV and 168.4 eV for **7b**, **8b**, and **9b**, respectively, can be related with sulfur present in sulfonate groups.[62-65] Similarly, deconvolution matching of the Au4f region (figure S33, supporting information) allows the localization of two peaks at 83.9 and 87.6 eV corresponding to the $Au4f_{7/2}$ and $Au4f_{5/2}$ levels, respectively, for all samples studied, that can be associated with the AuNP.[42, 65]

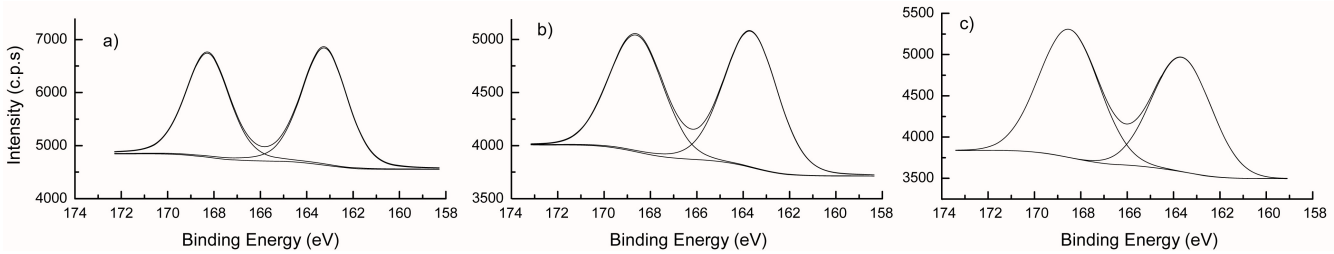

Figure 3. High resolution XPS spectra for the S2p region for a) Au@($SG_1(SO_3Na)_2$) (**7b**), b) Au@($SG_2(SO_3Na)_4$) (**8b**), and c) Au@($SG_3(SO_3Na)_8$) (**9b**).

The ^{1}H NMR spectra of these systems have resonances analogous to those of the dendrons, although clearly broadened. In the particular case of the methylene -CH_2SAu, this signal was not observed due to its proximity to the gold surface. With respect to UV-vis spectroscopy (Figure S34), the plasmon resonance is detected at about 515 nm, although this band is weak due to the small size of the NPs. The Z potential of these AuNPs was measured in water and negative values were obtained (Table 1). In general, their high negative values indicate formation of stable NPs toward aggregation, except for AuNP **7a**. We have to note that in the case of dendrons **4-6** the Z potential could not be obtained due to their small sizes and

because the presence of the thiol at the focal point degraded the cell electrodes. The Z potential is not a direct measure of surface charge, but of the potential of the hydrodynamic shear, and hence it is difficult to correlate Z potential data with the ability of sulfonate groups to interact with the surrounding. However, the values observed in AuNPs **7**-**9** reflect some differences between these systems, which have been also detected in the interaction of AuNPs with Cu(II) ions and also in their antiviral activity.

Nanoparticles	Molar Ratio Au/S		D (nm)[a]	Molecular formula[b]	Av. MW ($gmol^{-1}$)[b]	N[c]	ZP (mV)
	Theoretic	Obtained					
Au@($SG_1(SO_3Na)_2$) **(7a)**	1:1	3.04:1	2.4	$Au_{427}(C_{15}H_{31}Na_2O_6S_5Si)_{140}$	159953	280	-22.8
Au@($SG_1(SO_3Na)_2$) **(7b)**	2:1	5.65:1	3.6	$Au_{1441}(C_{15}H_{31}Na_2O_6S_5Si)_{255}$	421978	510	-31.4
Au@($SG_2(SO_3Na)_4$) **(8b)**	4:1	10.01:1	3.4	$Au_{1214}(C_{33}H_{69}Na_4O_{12}S_9Si_3)_{121}$	374956	484	-29.1
Au@($SG_3(SO_3Na)_8$) **(9b)**	8:1	20.16:1	3.0	$Au_{834}(C_{69}H_{145}Na_8O_{24}S_{17}Si_7)_{41}$	257929	328	-40.1
Au@($SG_1(SO_3Na)_2$)(SC12) **(7c)**			1.2				-57.0
Au@($SG_2(SO_3Na)_4$)(SC12) **(8c)**			1.8				-30.1
Au@($SG_3(SO_3Na)_8$)(SC12) **(9c)**			1.0				-63.9

Table 1. Selected data of AuNP **7-9**. a) Obtained by TEM; b) Obtained by TGA and elemental analysis; c) Number of sulfonate groups by NP.

The second methodology to prepare AuNPs (place-exchange) used gold nanoparticles of about 2.8 nm of diameter capped with dodecanethiol (Au@SC12), which were prepared employing a Au:S molar ratio of 1:1 (see experimental part).[66] Next, Au@SC12 were mixed with a huge excess of dendrons $HSG_n(SO_3^-)_m$ (**4-6**) in a mixture of CH_2Cl_2/water. This afforded the corresponding anionic gold nanoparticles $Au@(SC12)_x(SG_n(SO_3^-)_m)_y$ (n = 1, m = 2 (**7c**); n = 2, m = 4 (**8c**); n = 3, m = 8 (**9c**)) after dialysis of the water solution (MWCO 10 KDa). The same procedure employing $HS(CH_2)_3SO_3^-$ did not give the corresponding NPs, probably due to the small size of this compound, which cannot displace the alkane ligand or stabilize the AuNPs. Compounds **7c-9c** were characterized by TEM, TGA, elemental analysis, ^{1}H NMR, UV-vis and Z potential (Table 1).

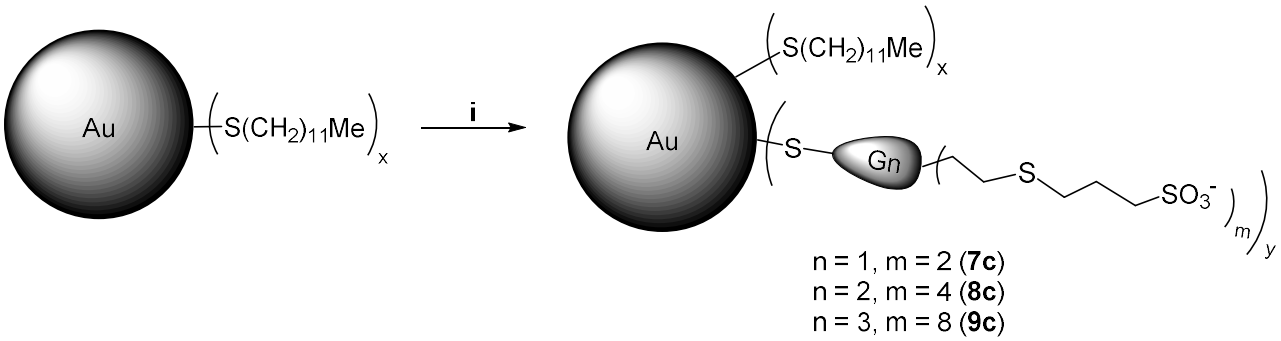

Scheme 3. Synthesis of anionic gold nanoparticles ($Au@(SC12)_x(SG_n(SO_3^-)_m)_y$) (**7c-9c**) by place-exchange reaction. i) $HSG_n(SO_3^-)_m$ (n = 1, m = 2 (**4**); n = 2, m = 4 (**5**); n = 3, m = 8 (**6**).

TEM images showed a decrease in size of the AuNPs **7c-9c** with respect to the precursor Au@SC12, principally for first and third generations. Moreover, with this procedure smaller NPs than those obtained by the direct synthesis were formed. TGA and elemental analysis did not enable us to differentiate the two types of ligands in AuNPs **7c-9c**. In the UV-vis spectra (Figure S34), the surface plasmon resonance for AuNPs **7c-9c** appeared as very weak signals around 515 nm, as consequence of their small sizes and as in related derivatives **7b-9b**. With respect to Z potential measurements, **7c** and **9c** presented clearly higher negative values when compared with the rest of anionic AuNPs described in this work. These data could indicate a higher crowding of the surface due to the smaller sizes of the NPs. Anyway, all these

compounds showed enough negative values that indicate presence of sulfonate functions on the NPs surface and that they are stable in solution toward aggregation.

In the ^{1}H-NMR spectra of compounds **7c-9c**, again the resonances corresponding to the methylene -CH_2SAu were not observed, being the rest of resonances clearly broadened with respect to the original signals in thiol ligands. Moreover, the resonances of the dodecanothiolate fragments are overlapped with those of the carbosilane framework. To calculate the relationship dendron:dodecanethiol, AuNPs were decomposed with I_2.[67] In this process three types of disulfur compounds, dendron-dendron, dendron-dodecyl and dodecyl-dodecyl can be released. The treatment of the reaction mixture (supporting information) and further comparative integration of region at ca. δ 1.30, which comprised the resonances for the dodecyl methylenes and for the central methylenes of $SiCH_2CH_2CH_2Si$ chains, with respect to the region at ca. δ 2.90, which belongs to the methylene CH_2SO_3 of dendrons, allowed us to obtain the dendron:dodecanothiol ratio: 12.5:1 for **7c** and **8c** and 7.7:1 for **9c**.

2.3 Cu^{II} as a probe of the structure and complexing ability of dendrons $HSG_n(SO_3^-)_m$ and AuNPs ($Au@(SG_n(SO_3^-)_m)$)

^{1}H-NMR spectra seem to indicate that formation of AuNPs proceeded by capping gold with the thiol at the focal point. However, the coordination ability of thioether and sulfonate functions in dendrons could compete with this focal point and hamper formation of the desired type of AuNPs, as commented above. For example, sulfonate thioether-carbosilane dendrimers have been used to stabilize AgNPs.[68] We have previously studied by EPR the ability of peripheral sulfonate groups to coordinate Cu^{II} cations in anionic carbosilane dendrimers, the coordination mode being dependent upon the SO_3^-/Cu^{II} molar ratio.[56, 57] With this in mind and the aim to confirm the type of interaction between gold surface and dendrons, we researched dendrons $HSG_n(SO_3^-)_m$ (**4-6**) and nanoparticles $Au@(SG_n(SO_3^-)_m)$ (**7a**, **7b-9b**) by using a computer aided analysis of the EPR spectra obtained by adding Cu^{II} at increasing amounts with respect to a fixed amount of sulfonate groups (0.01 M). Control spectra obtained by taking constant the copper(II) concentration and changing the nanocomposite concentration showed that the spectra were almost

comparable at the same Cu^{II}/SO_3^- group molar ratio, which is therefore the most relevant parameter in the system.

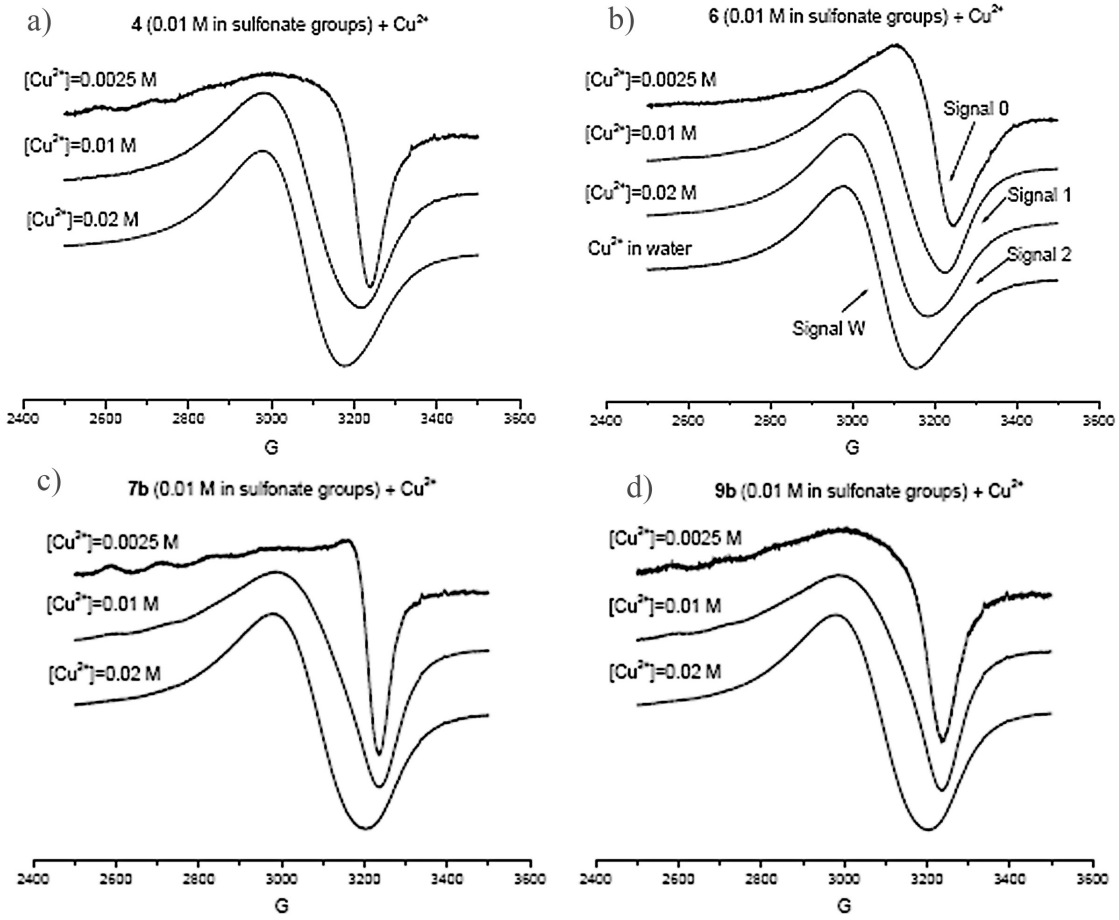

Figure 4. Selected EPR spectra obtained at 150 K for the samples: a) $HSG_1(SO_3^-)_2$ (**4**), b)$HSG_3(SO_3^-)_8$ (**6**), c) $Au@(SG_1(SO_3^-)_2)$ (**7b**), d) $Au@(SG_3(SO_3^-)_8)$ (**9b**).

Figure 4 shows, as informative examples, some selected EPR spectra obtained at 150 K for dendrons $HSG_1(SO_3^-)_2$ (**4**) (Figure 4a) and $HSG_3(SO_3^-)_8$ (**6**) (Figure 4b) and nanoparticles $Au@(SG_1(SO_3^-)_2)$ (**7b**) (Figure 4c) and $Au@(SG_3(SO_3^-)_8)$ (**9b**) (Figure 4d). All the spectra were recorded at different temperatures to follow the dynamics of the systems, but the spectra were computed at 298 K and 150 K. As apparent from the spectra, several components constitute the spectra of which main features are indicated with arrows in the spectra for the dendron **6**. Indeed, the components indicated as Signal 0 and Signal 2 are only present for second and third generation dendrons **5** and **6**, while all the samples gave the other two

components, termed Signal 1 and Signal W. This latter Signal corresponds to water-Cu^{II} complex, which is not informative about the Cu^{II} complexes with dendrons and AuNPs. By applying the subtraction process described above, the four components were extracted. Figure S35a (Supporting Information) shows the computations of Signal 0, Signal 1 and Signal 2 at 150 K. The magnetic parameters used for the computations of the different signals are reported in Table 2.

Spectral Component	g_{xx}	g_{yy}	g_{zz}	A_{xx} (G)	A_{yy} (G)	A_{zz} (G)	LW (G)
Signal 0	2.017	2.096	2.328	-8	-8	160	40
Signal 1	2.065	2.095	2.398	-8	-8	125	30
Signal 2	2.079	2.154	2.322[#]	-5	-20	116[#]	70

[#]very low accuracy, due to the poor resolution of this signal in the parallel region of gii and Aii

Table 2. Magnetic parameters used for computations of the signals constituting the spectra of copper(II) complexed by dendron **6**.

The parameters reported in Table 2 were compared with other magnetic parameters reported in the scientific literature for similar Cu^{II} complexes to identify the structure and coordination of the dendron complexes.[56, 57, 69, 70] All the Signals correspond to quite distorted square planar Cu^{II} coordination environments. Signal 1, which is well resolved for all the samples with the exception of **6**, is easily ascribed to a Cu-O4 coordination with sulfonate groups at the dendron surface; water molecules occupy the other coordination sites. Since Signal 1 is prevailing at low Cu^{II} concentrations, we hypothesize that two (or even more) sulfonate groups are involved in the complexation if the branch flexibility allows them to approach the ions. The lower resolution of Signal 1 in **6** may be ascribed to the superposition of several contributions from coordinations poorly differing from each other.

As shown in Figure 4, Signal 2 becomes evident only for **5** and **6** at molar ratios SO_3^-/Cu^{II} between 2:1 and 1:1 and it is a poorly resolved signal. The poor resolution, the low accuracy in the magnetic parameters and the high line width, and, finally, the molar ratio of existence, indicate a distribution of

coordinations due to the presence of several differently available sulfur containing groups, sulfonate and thiol. Dendron **4** is probably too small and does not allow different groups to contemporaneously approach the ions. Also, we did not find Signal 2 in the spectra of AuNPs **8b** and **9b**, as discussed later.

The magnetic parameters of Signal 0 were quite unexpected, since the high A_{zz} and the low g_{zz} are usually found when nitrogen atoms are included in the coordination sites. In this work, we do not have any other nitrogen site beyond the nitrate group, which is the Cu^{II} salt contra-ion. Since this signal appears for second and third generation dendrons **5** and **6** at the lowest Cu^{II} concentration and is absent at 298 K, we hypothesize the formation of dendron aggregates where the Cu^{II} ions work as bridges trapping inside the contra-ions as ligands of the ions.

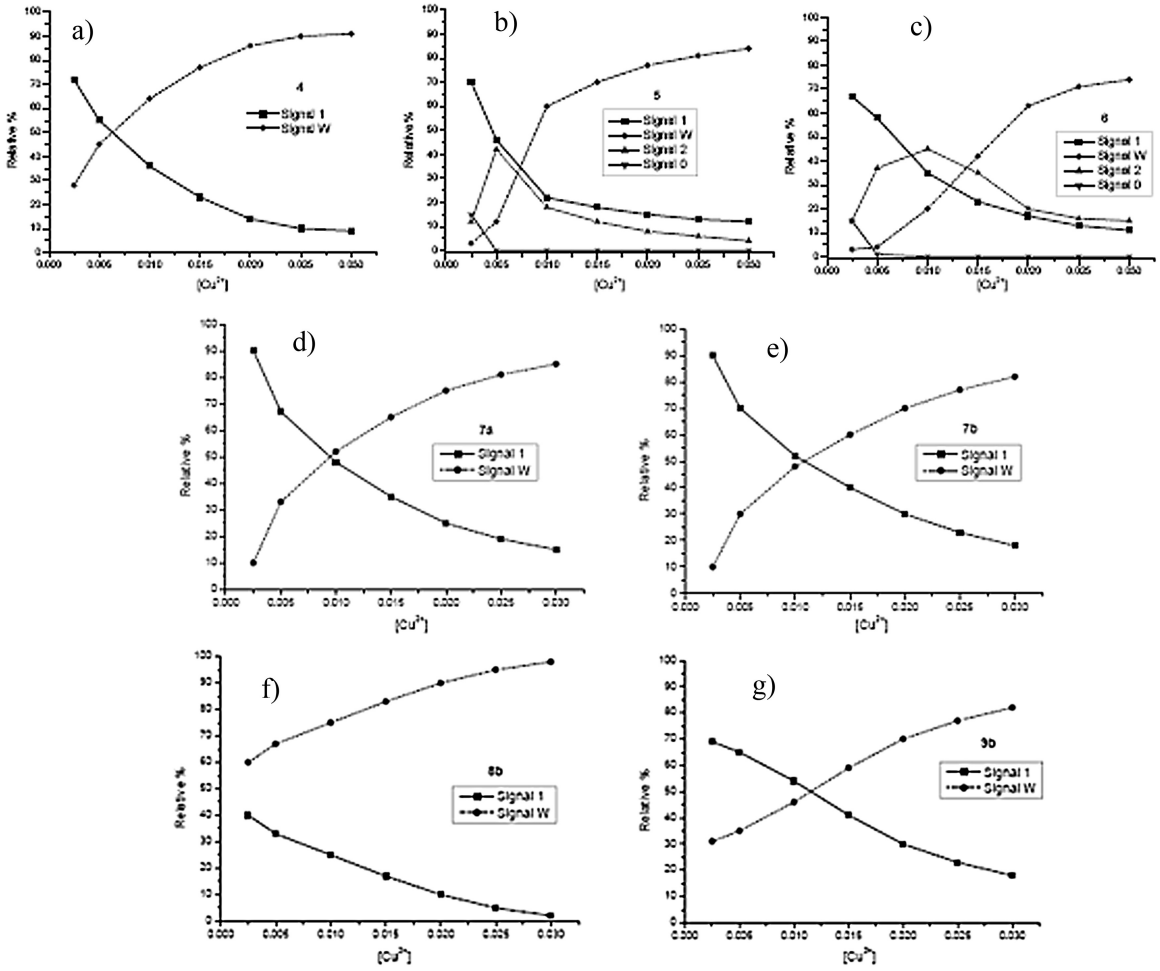

Figure 5. Relative percentages of the different signals constituting the EPR spectra at 150 K in function of copper(II) concentration for: a) **4**, b) **5**, c) **6**, d) **7a**, e) **7b**, f) **8b**, g) **9b**.

Further information was obtained by calculating the relative percentages of the spectral components for the various samples. The variations of the relative percentages of the different signals constituting the spectra at 150 K as a function of Cu^{II} concentration are reported in Figure 5 for **4** (a), **5** (b), **6** (c), **7a** (d), **7b** (e), **8b** (f), and **9b** (g). First, we note that significant modifications were apparent by increasing dendron generation from **4** to **6**, not only for the appearance of Signal 0 and Signal 2 for dendrons **5** and **6**, as has already been described above, but also because the different signals have different Cu^{II} ranges of appearance at different percentages. We first focalized our attention on Signal W, which appears and gains in relative percentage due to a progressive saturation of the dendron interacting sites. The most evident effect is that the higher the generation, the higher the Cu^{II} concentration at which this saturation takes place. This means that, the higher the generation, the higher the availability of sulfonate groups. It is also useful to underline the comparative behavior of Signal 1 in the pure dendrons, which indicates a lower availability of the sulfonate groups for **5** to complex the Cu^{II} ions if compared to **4** and **6**.

Some interesting and informative differences were found for the NPs $Au@(SG_n(SO_3^-)_m)$ if compared to the pure dendrons. AuNPs formed with G1 dendrons, **7a** and **7b**, both show a higher availability of the sulfonate sites to complexation if compared to the pure dendron **4**; for instance, at a SO_3^-/Cu^{II} molar ratio as low as 4, the pure dendron has 70 % of sulfonate complexes, while **7a** and **7b** have about 90 % of complexes. However, the sulfonate groups are a little bit less available for complexation in **7a** than in **7b**, probably due to a more crowd dendron organization in the former nanocomposite.

Regarding AuNPs with second generation dendrons **8b**, the situation completely reverses with respect to **7b**. At a SO_3^-/Cu^{II} molar ratio of 4, only 40 % of the ions are involved in the complexation with the sulfonate groups while the others are extruded in water. So, for **8b**, the availability of the sulfonate groups is quite poor. This may be again related to the structure/conformation of the dendrons by themselves and at the gold surface. We have to remember here, as discussed above, that the pure G2 dendron **5** showed a lower availability of the sulfonate groups to form the complex (Signal 1) if compared to dendrons **4** and **6**. This effect is enhanced for the AuNPs, where the complexes responsible of Signals 0 and 2 could not form any more, and only Signal 1 is observed. The absence of Signal 0 in the nanocomposites is quite obvious

since dendron aggregates cannot be formed. But also Signal 2 disappears in the nanocomposites **8b** and **9b**. This effect may arise from two sources. First, the binding of the dendron to Au in the AuNPs subtracts binding sites to Cu^{II} complexation. This strongly indicates that the complexation giving rise to Signal 2 involves the -SH groups at the focal point of dendrons. In line with this hypothesis, we have already found in past studies using sulfonate carbosilane dendrimers the absence of Signal 2.[69] Second, in **8b** and **9b** cases, the sulfonate groups may lose their ability to form "disordered" complexes like those responsible of Signal 2 probably due to packing of the dendrons. These AuNPs are only able to form the Cu-O4 coordination responsible of Signal 1. However, in **9b**, the availability of the sulfonate groups for forming Signal 1 is recovered with respect to **8b**, as already found for **6** with respect to **5**, due to the structure of these dendrons.

2.4 Cytotoxic effect and antiviral properties of dendrons and dendronized AuNPs

In order to determine if dendrons and AuNPs are valid candidates for their use in a potential anti-HIV microbicide formulation, we evaluated the toxic effect using a well-established metabolic activity assay (MTT). Dendrons (**4-6**) and AuNPs obtained from both procedures (**7b-9b** and **7c-9c**) were tested on TZM.bl cells in the range 0.01 to 20 μM and 0.01 to 100 μg/ml at 24 h and 48 h of treatment, respectively (Figure 6 and Figure S36). Concentrations in which the cellular viability was above 80% compared to control cultures were considered non-toxic. First and second generation dendrons **4** and **5** were non-toxic at maxim concentration of 20 μM, whilst third generation derivative **6** was toxic at all concentrations. Thus, we ruled out it for inhibition assays. With respect to NPs, the toxicity of the systems decorated only with sulfonate dendrons Au@(SGn$(SO_3Na)_m$) (**7b-9b**) were lower than the toxicity of NPs containing also dodecanothiol ligands (Au@$(SC12)_x(SG_n(SO_3^-)_m)_y$) (**7c-9c**) (Figure S36). Au@(SG1$(SO_3Na)_2$) (**7b**) was non-toxic at 10 μg/ml, Au@(SG2$(SO_3Na)_4$) (**8b**) at 1 μg/ml and Au@(SG3$(SO_3Na)_8$) (**9b**) at 0.5 μg/ml, whereas toxicity levels for NPs **7c-9c** were below 0.1 μg/ml. Clearly, this result can be ascribed to the remaining long alkyl chains in NPs **7c-9c**. In addition, the biocompatibility of AuNPs **7b-9b** was evaluated in peripheral blood mononuclear cells (PBMC) at 48 h of exposure in the range 1-100 μg/ml. All

concentrations showed values over 95% of viability. Therefore, 100 µg/ml was chosen as non-toxic concentration for PBMC.

The effect of dendronization can be noticed if the data are compared with respect to dendron concentration, as free dendrons **4-6** or as ligands covering the NPs surface (Figure S37, supporting information). This comparison of toxicity values brings out that dendrons of first and second generation are less toxic by themselves than in NPs, whereas third generation derivative is slightly less toxic when capping the NPs.

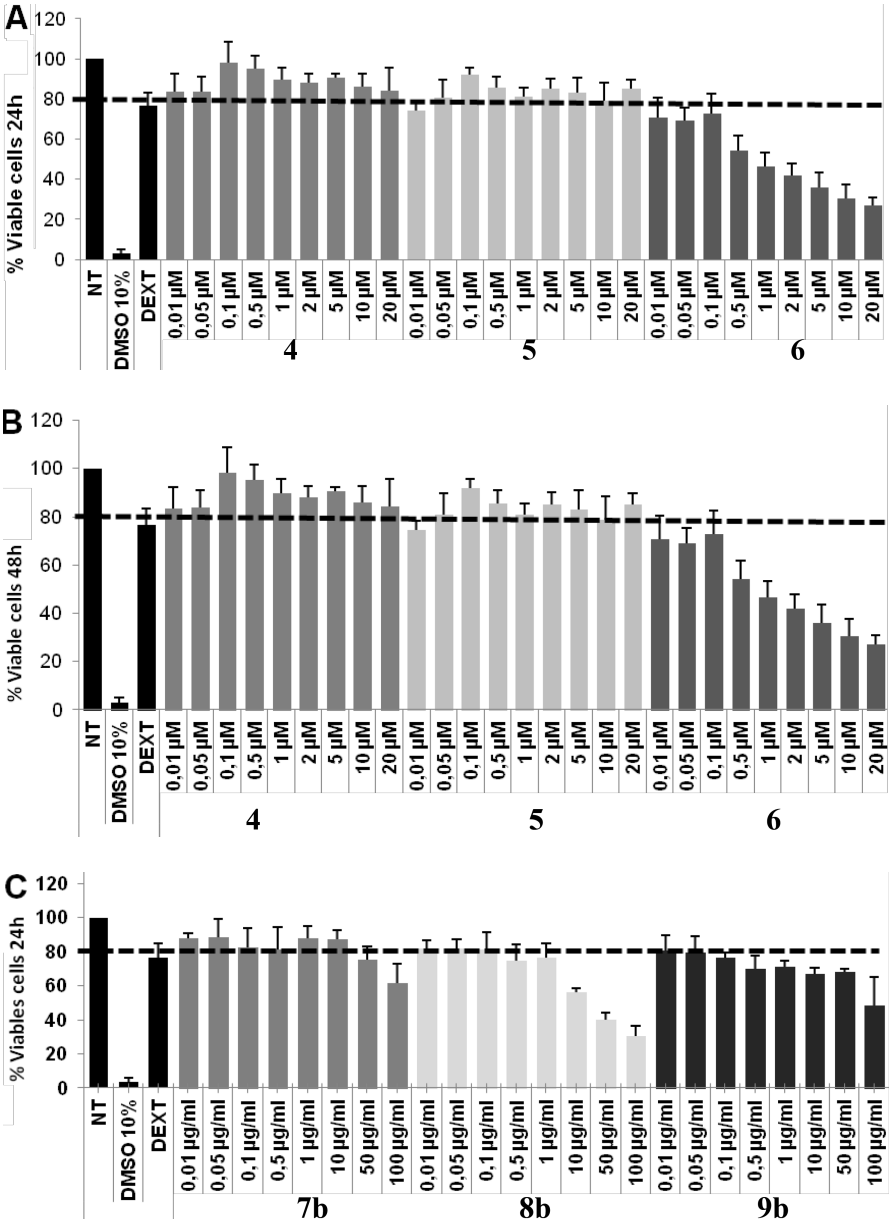

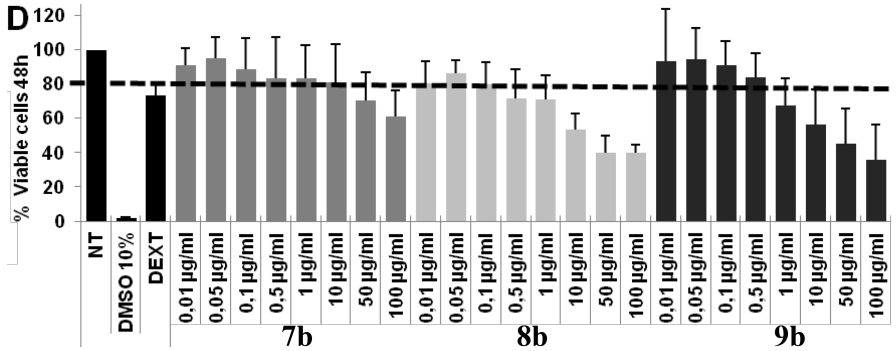

Figure 6. Toxicity of anionic dendrons and NPs. TZM.bl cells were treated in the presence of a range of concentrations from 0.01 µM to 20 µM of dendrons and 0.01 µg/ml to 100 µg/ml of AuNPs for 24 h (A, C) or 48 h (B, D). Dextran 10 µM was used as negative control of cellular death (non toxic compounds) and DMSO 10% was used as positive control of toxicity. The discontinuous line corresponds to 80% of viability set as limit of toxicity for viable cells. Data represent the mean ± SEM (n=3).

Dendrons and NPs were tested against R5-HIV-1 and X4-HV-1 isolates using TZM-bl cells in which infection was quantified by a luciferase-based assay (Figure 7). Replication inhibition of X4-HIV isolates *in vitro* was observed for first and second generation dendrons **4** and **5**, whilst inhibitory effect against R5-HIV-1 isolate was only observed for second generation dendron **5**. Regarding AuNPs, only were studied the compounds obtained by the direct procedure, **7b-9b**, due to their higher biocompatibility. These systems inhibited both isolates with similar pattern. The concentration at which inhibition was higher than 80% was above 0.5 µg/ml and 0.1 µg/ml for NPs capped with dendrons of first and third generation **7b** and **9b**, respectively. The second generation Au@(SG2($SO_3Na)_4$ (**8b**) showed lower ability to inhibit infection, requiring concentrations above 1 µg/ml. These assays highlight the relevance of dendronization, since anionic NPs inhibit both HIV isolates but free dendrons are only partially active against X4-HIV-1.

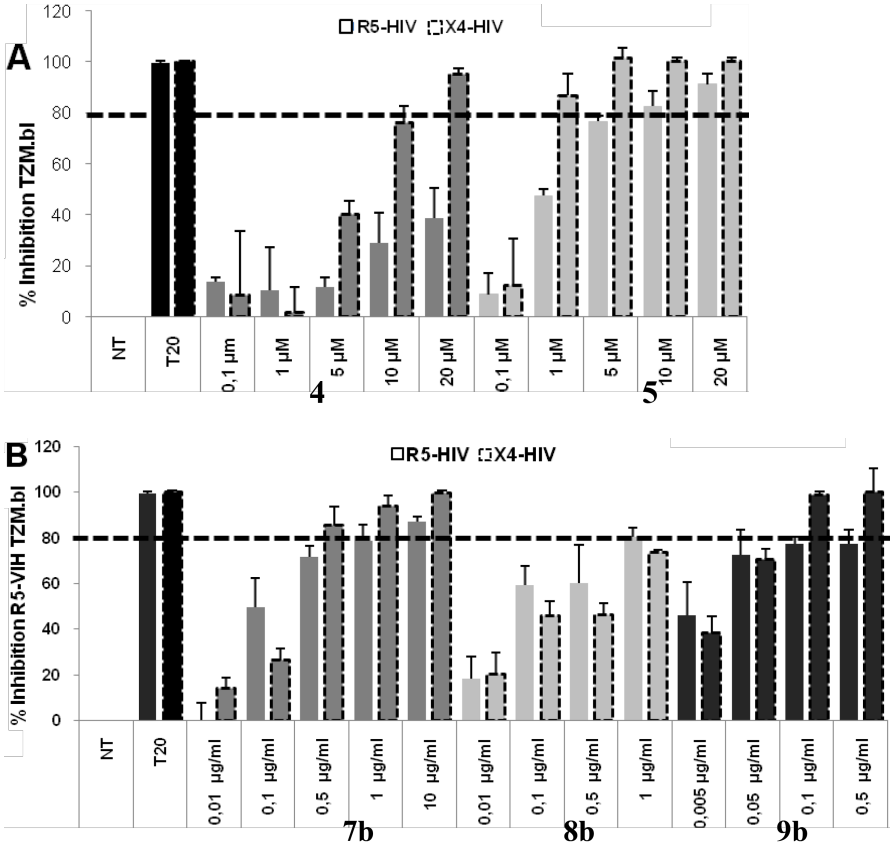

Figure 7. Inhibition of R5-HIV-1_{NLAD8} and X4-HIV-$1_{NL4.3}$ infections in TZM.bl cells by dendrons HSG1$(SO_3Na)_2$ (**4**) and HSG2$(SO_3Na)_4$ (**5**) and NPs Au@(SG1$(SO_3Na)_2$) (**7b**), Au@(SG2$(SO_3Na)_4$) (**8b**), and Au@(SG3$(SO_3Na)_8$) (**9b**). TZM.bl cells were pretreated with increased non-toxic concentrations of dendrons **4** and **5** (A) and NPs **7b-9b** (B), 1 h before HIV-1 infection with R5-HIV-1_{NLAD8} or X4-HIV-$1_{NL4.3}$ isolates at a concentration 50 ng/10^6 cells. TZM.bl cells were lysed and HIV-1 replication was determined at 72 h by quantification of luciferase expression. Antiviral T20 (enfuvirtide, fusion inhibitor) 20µM was used as positive control of the inhibition of HIV-1 infection. The discontinuous line corresponds to 80 % of inhibitory effect on VIH-1 infection. Data represent the mean ± SEM (n=3).

3. Conclusions

Anionic carbosilane dendrons with –SH function at the focal point and $–SO_3^-$ groups at the periphery were used to stabilize gold nanoparticles by reaction of the dendrons with the gold precursor ($[AuCl_4]^-$) and the reducing agent ($NaBH_4$) in water (Brust-Schriffin method) or also by place-exchange reaction from previously isolated AuNPs protected with dodecanethiol (Au@SC12). For the Brust-Schriffin

method, the presence of extra sulfur atoms in dendrons and the coordinating ability of the $S(CH_2)_3SO_3^-$ moiety that could hinder gold aggregation require the use of high Au/dendron ratios to form NPs, mainly for second and third generations. In both cases, the AuNPs obtained were soluble in water and stable for long periods of time. In contrast, when analogous processes were carried out for the monofunctionalized sulfonate derivative $HS(CH_2)_3SO_3^-$, no stable AuNPs could be isolated. The AuNPs were characterized by TEM, TGA, elemental analysis, XPS, ^{1}H NMR, UV, Z potential, and EPR. EPR analysis of dendrons and AuNPs at variable Cu^{II} concentrations indicate a similar availability of sulfonate groups to complex Cu^{II} ions in both type of systems, and hence, helping to confirm that AuNPs are formed by capping with the sulfur atom of the focal point. For the dendrons, the thiol at the focal point is also participating to the Cu^{II} complexation in second and third generation dendrons. However, AuNPs functionalized with second generation dendrons showed slightly lower coordination ability that could be related with some degree of backfolding to minimize charge repulsions.

The antiviral activities of dendrons and AuNPs against HIV-1 at non-cytotoxic concentrations in TZM.bl cells indicate that dendrons by themselves have lower efficiency than AuNPs. High activity of AuNPs is suggested to be due to their lower citotoxicity. In the particular case of $Au@(SG2(SO_3Na)_4$ (**8b**), the lower exposure of sulfonate groups in this system due to backfolding led to a small diminution of their antiviral activity. Regarding HIV-1 strains, AuNPs inhibited both of them, although those capped with second and third generation dendrons, **8b** and **9b**, have higher inhibitory activity against R5-tropic HIV-1 isolate than against X4-tropic HIV-1 isolate.. The mode of action of AuNPs does not depend on this determinant of cell tropism. Hence, the results obtained emphasize the relevance of dendronization, because the toxicity is diminished and the antiviral activity is increased with respect to the pioneer dendron compounds. However, it would be necessary different *in vitro* assays for elucidating their mode of antiviral action against HIV-1 as well as in which stage of viral replication.

4. Experimental Section

4.1. General Considerations. All reactions were carried out under inert atmosphere and solvents were purified from appropriate drying agents when necessary. Thiol-ene reactions were carried out employing a HPK 125W Mercury Lamp from Heraeus Noblelight with maximum energy at 365 nm, in normal glassware under inert atmosphere. NMR spectra were recorded on a Varian Unity VXR-300 (300.13 (^{1}H), 75.47 (^{13}C) MHz) or on a Bruker AV400 (400.13 (^{1}H), 100.60 (^{13}C), 79.49 (^{29}Si) MHz). Chemical shifts (δ) are given in ppm. ^{1}H and ^{13}C resonances were measured relative to solvent peaks considering TMS = 0 ppm, meanwhile ^{29}Si resonances were measured relative to external TMS. When needed, assignment of resonances was done from HSQC, HMBC, COSY and TOCSY NMR experiments. Elemental analyses were performed on a LECO CHNS-932. Mass Spectra were obtained from a Bruker Ultraflex III for MALDI-TOF in dithranol, an Agilent 6210 TOF LC/MS for ESI-TOF in MeOH/H_2O with $(NH_4)(HCO_2)$, and an AB Sciex QSTAR for ESI-POS in H_2O/MeOH. Compounds $HS(CH_2)_3SO_3Na$, 2,2'-dimethoxy-2-phenylacetophenone (DMPA), $NaAuCl_4$, $NaBH_4$ were obtained from commercial sources. Compounds $(MeCOS)G_nV_m$ (n = 1, m = 2; n = 2, m = 4; n = 3, m = 8)[50] were synthesized as previously published.

4.2. Synthesis of compounds.

In this section are described the preparation of first generation dendrons and AuNPs. The complete descriptions of all compounds are collected in Supporting Information.

$MeCOSG_1(SO_3Na)_2$ (1). An aqueous solution of $HS(CH_2)_3SO_3Na$ (1.059 g, 5.942 mmol) was added to a THF solution of **$MeCOSG_1V_2$** (5.943 g, 2.913 mmol) in the presence of DMPA (10%) and stirred under ultraviolet light for 4 h. Volatiles were removed under vacuum, the residue was dissolved in H_2O and excess of Et_2O was added, the precipitate was washed with Et_2O, yielding **1** as a yellow solid (1.19 g, 70 %). Data for **1**: NMR (D_2O): ^{1}H NMR: δ -0.05 (s, 3 H, SiC*H*$_3$), 0.53 (m, 2 H, $SCH_2CH_2CH_2CH_2Si$), 0.84 (m, 4 H, $SiCH_2CH_2S$), 1.31 (m, 2 H, $SCH_2CH_2CH_2CH_2Si$), 1.52 (m, 2 H, $SCH_2CH_2CH_2CH_2Si$), 1.92 (m, 4 H, $SCH_2CH_2CH_2S$), 2.27 (s, 3 H, CH_3COS), 2.58 (m, 8 H, $SiCH_2CH_2S$, $SCH_2CH_2CH_2S$), 2.82 (m, 2 H, $MeCOSCH_2$), 2.93 (m, 4 H, CH_2SO_3); ^{13}C NMR{^{1}H}: δ -5.6 ($SiCH_3$), 12.7 ($SCH_2CH_2CH_2CH_2Si$), 14.1 ($SiCH_2CH_2S$), 22.6 ($SCH_2CH_2CH_2CH_2Si$), 24.1 ($SCH_2CH_2CH_2S$), 26.8 ($SiCH_2CH_2S$) 28.7 ($MeCOSCH_2$), 29.9 ($SCH_2CH_2CH_2S$), 30.4 (CH_3COS), 32.6 ($SCH_2CH_2CH_2CH_2Si$), 50.1 ($SCH_2CH_2CH_2S$), 199.0

(CH_3COS); ^{29}Si NMR: δ 2.8 ($SiCH_3$). MS $[M - 2\ Na^+]^-$ = 539.08. Adequate analytical data could not be obtained for this compound because the size and solubility of final product was close to the starting $HS(CH_2)_3SO_3Na$.

$HSG_1(SO_3Na)_2$ (4). HCl in ether (2 M, 5.1 mL, 10.20 mmol) was added to a MeOH solution of **1** (0.993 g, 1.697 mmol) and the mixture was stirred at 55°C overnight. Afterward, volatiles were removed under vacuum yielding **4** as a yellowish solid (0.878 g, 95 %). Data for **4**: NMR (D_2O): ^{1}H NMR: δ -0.07 (s, 3 H, $SiCH_3$), 0.53 (m, 2 H, $SCH_2CH_2CH_2CH_2Si$), 0.83 (m, 4 H, $SiCH_2CH_2S$), 1.32 (m, 2 H, $SCH_2CH_2CH_2CH_2Si$), 1.52 (m, 2 H, $SCH_2CH_2CH_2CH_2Si$), 1,90 (m, 4 H, $SCH_2CH_2CH_2S$), 2.55 (m, 10 H, $SiCH_2CH_2S$, $SCH_2CH_2CH_2S$, $HSCH_2CH_2CH_2CH_2Si$), 2.89 (M, 4 H, $SCH_2CH_2CH_2S$); ^{13}C NMR{^{1}H}: δ -6.3 ($SiCH_3$), 11.9 ($SCH_2CH_2CH_2CH_2Si$), 13.6 ($SiCH_2CH_2S$), 22.4 ($HSCH_2$), 24.0 ($SCH_2CH_2CH_2S$), 24.3 ($SCH_2CH_2CH_2CH_2Si$), 26.8 ($SiCH_2CH_2S$), 29.3 ($SCH_2CH_2CH_2S$), 31.7 ($SCH_2CH_2CH_2CH_2Si$), 49.8 ($SCH_2CH_2CH_2S$); ^{29}Si NMR: δ 2.7 ($SiCH_3$). MS $[M - 2\ Na^+]^-$ = 496.5. Adequate analytical data could not be obtained for this compound because the final product showed a behavior very close to the starting $HS(CH_2)_3SO_3Na$.

Au@($SG_1(SO_3Na)_2$) (7a). An aqueous solution of compound **4** (26.6 mL, 0.3 mmol, 12.5 mM) was added dropwise to an aqueous solution of $HAuCl_4$ (10 mL, 0.3 mmol, 30 mM). Afterward, $NaBH_4$ in water (7.5 mL, 1.5 mmol, 200 mM) was added dropwise, and the mixture was stirred another 4 h. Nanoparticles were purified by dialysis (MWCO 10,000) affording **7a** (200 mg, stored in deionized water at 4 ºC). Data for **7a**: NMR (D_2O): ^{1}H NMR: δ 0.06 ($SiCH_3$), 0.61 ($SCH_2CH_2CH_2CH_2Si$), 0.89 ($SiCH_2CH_2S$), 1.93 ($SCH_2CH_2CH_2S$), 2.60 ($SiCH_2CH_2S$, $SCH_2CH_2CH_2S$), 2.90 ($SCH_2CH_2CH_2S$). Au/(l) reactant molar ratio = 1:1. Anal. Obt.: C, 21.36; H, 4.12; S,18.17. TGA: Au, 52.47; (l), 47.53. Calc. molar ratio Au/(l) = 3.04:1 in the nanoparticles. Zeta potential (mV): -22.8. Mean diameter of gold core (TEM): D = 2.4 nm. N_{Au} = 427; N_{th} = 140. Molecular weight calculation: $Au_{427}(C_{15}H_{31}Na_2O_6S_5Si)_{140}$. Average M = 159953 gmol^{-1}.

Au@($SG_1(SO_3Na)_2$) (7b). Following the procedure described for compound **7a**, compound **7b** was obtained (262 mg) from the reaction of $HAuCl_4$ (10 mL, 0.3 mmol, 30 mM) with compound **5** (24 mL,

0.15 mmol, 6.25 mM) and $NaBH_4$ (7.5 mL, 1.5 mmol, 200 mM) Nanoparticles were purified by dialysis (MWCO 10,000) Data for **7b**: NMR (D_2O): ^1H NMR: δ 0.07 ($SiCH_3$), 0.62 ($SCH_2CH_2CH_2CH_2Si$), 0.90 ($SiCH_2CH_2S$), 1.91 ($SCH_2CH_2CH_2S$), 2.59 ($SiCH_2CH_2S$, $SCH_2CH_2CH_2S$), 2.90 ($SCH_2CH_2CH_2S$). Au/(l) reactant molar ratio = 2:1. Anal. Obt.: C, 21.79; H, 4.35; S,18.56. TGA: Au, 67.28; (l), 32.71. Calc. molar ratio Au/(l) = 5.65:1 in the nanoparticles. Zeta potential (mV): -31.4. Mean diameter of gold core (TEM): D = 3.6 nm. N_{Au} = 1441; N_{th} = 255. Molecular weight calculation: $Au_{1441}(C_{15}H_{31}Na_2O_6S_5Si)_{255}$. Average M = 421978 $gmol^{-1}$.

Au@($SG_1(SO_3Na)_2$)(SC12) (7c). An aqueous solution of compound **4** (129 mg, 0.239 mmol) in deionized water (10 mL) was added to a solution of compound **Au@(SC12)** (10 mg) in dichloromethane (10 mL) under argon. The mixture was stirred at room temperature until the end of the ligand exchange (the exchange of ligands can be easily observed by the transfer of dark color from the organic phase to the aqueous phase). Upon complexion of exchange reaction the layers were separated, and the aqueous layer was washed with dichloromethane (2 x 5 mL). Afterwards, the aqueous phase was evaporated and the obtained residue was purified by dialysis yielding **7c** (127 mg, stored in water solution at 4 ºC). Data for **7c**: NMR (D_2O): NMR (D_2O): ^1H NMR: δ -0.01 (m, $SiCH_3$), 0.54 (m, $SCH_2CH_2CH_2CH_2Si$), 0.85 (m, $SCH_2(CH_2)_9CH_3$, $SiCH_2CH_2S$), 1.37 (m, $SCH_2(CH_2)_9CH_3$, $SCH_2CH_2CH_2CH_2Si$), 1.59 (m, $SCH_2CH_2CH_2CH_2Si$), 1.92 (m, $SCH_2CH_2CH_2S$), 2.58 (m, $SiCH_2CH_2S$, $SCH_2CH_2CH_2S$, $SCH_2CH_2CH_2CH_2Si$), 2.89 (m, $SCH_2CH_2CH_2S$). Anal. Obt.: C, 34.12; H, 6.93; S, 26.01. TGA: Au, 39.68; (l), 60.33. Zeta potential (mV): -57. Mean diameter of gold core (TEM): D = 1.2 nm.

4.3 UV-vis optical Spectroscopy. The UV-visible absorption measurements were performed using a Perkin-Elmer Lambda 18 spectrophotometer. The spectra were recorded by measuring dilute samples in a quartz cell with a path length of 1 cm.

4.4 Thermogravimetric Analysis (TGA). The thermogravimetrics analyses were performed using a Q500 from TGA instruments. Dry and pure samples (2 - 10 mg) were placed into platinum sample holder under nitrogen atmosphere. The measurements were recorded from 25 to 1000 ºC, with heating rate of 10 ºC/min.

4.5 Transmission electron microscopy (TEM). TEM were performed using a ZEISS EM10 TEM with 30 μm lens and a side-mounted 1K CCD Camera, operating at an acceleration voltage of 100 kV and with 0.2 nm resolution. The samples were prepared by dropping a dilute solution containing the nanoparticles on a carbon-coated copper grid (400 mesh) and dried before observation and measurement (particles size measurements were performed using Image J).

4.6 X-ray photoelectron spectroscopy (XPS). XPS analyses were performed using a K-Alpha (Thermo Scientific) system, with monochromatic AlKα (1486.68 eV) X-ray source with a spot size of 200 μm and 50.4 W (12 kV × 4.2 mA) power. AuNP-dendron solutions were drop-cast onto aluminum foil for analysis. High resolution and survey spectra were collected at three positions for each sample. The XPS spectra were background subtracted using the Shirley method and deconvoluted using a mixed Gaussian/Lorentzian peak shape with XPSPeak software (version 4.1).

4.7 Zeta Potential.

The zeta-potential of compounds were measured using a Zetasizer Nano ZS (Malvern Instruments Ltd., UK) at 25 ºC in a disposable Malvern plastic cuvette. The solutions were prepared by solving 1 mg of each compound in 1 mL of purified water, which was previously filtered through 0.22 μm syringe filter.

4.8 Electronic paramagnetic resonance (EPR). EPR spectra were recorded by means of an EMX-Bruker spectrometer operating at X band (9.5 GHz) and interfaced with a PC (software from Bruker for handling the EPR spectra). The temperature was controlled with a Bruker ST3000 variable-temperature assembly cooled with liquid nitrogen. For the EPR analysis, the nanoparticles were dissolved in millipore doubly distilled water resulting in a final external sulfonate groups concentration of 0.1 M. Cupric nitrate hydrate ($Cu(NO_3)_2 \cdot 2.5H_2O$, Sigma- Aldrich, ACS reagent 98 %) was also dissolved in millipore doubly distilled water to obtain a final concentration, in the mixture with the nanoparticles, from 0.1 to 5 equivalents. The Cu^{II}/sulfonate molar ratio was changed holding constant the concentration of the dendron or, alternatively, that of Cu^{II}. The samples were left equilibrating from 1 to 24 h (we verified that the spectra did not change in this time range). The EPR tubes have a constant internal diameter of 2 mm and were filled with 50 μL of solution. The EPR spectra were recorded for the different samples as a function

of temperature, but the spectra were only computed at 298K and 150 K. In all cases, we controlled the reproducibility of the results by repeating the EPR analysis (three times) in the same experimental conditions for each sample. Computation of the spectra was performed by using the well-established procedure of Budil and Freed,[71] which allowed us to also evaluate the dynamics of the system. Indeed, the main parameters obtained from computation were: (i) the g_{ii} components for the coupling between the magnetic field and the electron spin (accuracy ± 0.001). As internal reference having <g> = 2.0036, 1,1-diphenyl-2-picryl-hydrazyl (DPPH) standard was added to the solutions. The accuracy in this parameter is ± 0.0001; (ii) the A_{ii} components for the coupling between the electron spin and the Cu (II) nuclear spin (I=3/2). The accuracy in this parameter is ± 0.5 G; (iii) the line width, indicated as LW (accuracy ± 0.5 G); and (iv) for the spectra at 298 K, the correlation time for the rotational motion of the Cu^{II} ions, indicated with τ (accuracy ± 0.01 ns). In almost all cases, the spectra are constituted by different Signals, that is, different components corresponding to Cu^{II} in different coordination sites. A subtraction procedure from one to another experimental spectrum allowed us to extract the different components, to quantify them by means of a double integration of the signals, to evaluate the relative percentages (accuracy ± 1 %), and to separately compute the different components to extract the structural and dynamical information.

4.9 Cell cultures.

TZM.bl cell line (NIH AIDS Research and Reference Reagent Program) is derived from HeLa cell line which contains integrated copies of the luciferase and β-galactosidase genes under control of the HIV-1 promoter.[72] TZM.bl cells express large amounts of CD4 and CCR5. TZM-bl cells were cultured in DMEM (Life Technologies, Spain) supplemented with 5% heat-inactivated FBS, 2 mM L-glutamine and antibiotic cocktail (125 mg/ml amphicilin, 125 mg/ml cloxaciclin and 40 mg/ml gentamicin; Sigma-Aldrich, St-Louis, MO, USA). Peripheral blood mononuclear cells (PBMC) were isolated with standard Ficoll gradient from buffy coats (Rafer, Spain) and cultured as already described.[73]

4.10 Viruses.

CCR5-tropic R5-HIV-$1_{NL(AD8)}$ and CXCR4-tropic X4-HIV-1_{NL4-3} laboratory strains were obtained by transient transfection of pNL(AD8) and pNL4-3 plasmids, respectively (NIH AIDS Research and

Reference Reagent Program) in 293T cells (ATCC, Manassas. VA, USA). Viral stocks were clarified by centrifugation prior to evaluate the viral titer by HIV-1p24^{gag} ELISA kit (INNOTEST® HIV AntigenmAb, Innogenetics, Belgium).

4.11 Cell viability assays.

Gold nanoparticles toxicity was determined by 3-(4,5-dimethylthiazol-2-yl)-2,5-diphenyltetrazolium bromide (MTT) (Sigma-Aldrich, St Louis, Missouri, USA) assay according of manufacturer´s instructions. DMSO 10% (Sigma-Aldrich) was used as positive control of cellular death and dextran 10 μM were used as negative control. Each experiment was performed by triplicate.

4.12 Inhibition of HIV-1 replication experiments.

Pre-treatment assay: TZM.bl cells were seeded in p96 well plates 24 h prior to the experiment (15 x 10^3/200μl). After 1 h of pre-treatment with different concentrations of non toxic AuNPs, cells were infected for 3 h with R5-HIV-$1_{NL(AD8)}$ or X4-HIV-$1_{NL4.3}$ (50 ng/10^6 cells) in culture conditions. Then, cells were washed twice with PBS and incubated 72 h at 37 ºC and 5 % CO_2. After this time, cells were lysed and HIV-1 replication was determined by quantification of luciferase expression (Luciferase Assay System, Promega) according to kit protocol. T20 (fusion inhibitor) at a concentration of 20 μM was used as positive control of the inhibition of HIV-1 infection. Each experiment was performed by triplicate.

5. Acknowledgments.

This work has been supported by grants from CTQ2011-23245, CTQ-2014-54004-P (MINECO), and Consortium NANODENDMED ref S2011/BMD-2351 (CAM) to University of Alcalá, by the RD12/0017/0037 project as part of the Acción Estratégica en Salud, Plan Nacional Investigación Científica, Desarrollo e Innovación Tecnológica 2008-2011 and cofinanced by Instituto de Salud Carlos III (Subdirección General de Evaluación) and Fondo Europeo de Desarrollo Regional (FEDER), RETIC PT13/0010/0028, (FIS) (grant number PI13/02016), Comunidad de Madrid (S-2010/BMD-2332], CYTED 214RT0482. The XPS has been performed by NANBIOSIS ICTS, more specifically by the Surface Characterization Unit of the Biomedical Networking Center (CIBER-BBN) and the SACSS- SAIUEx of

the University of Extremadura (UEx). M. F. O. acknowledges financial support from Italian PRIN2012-NANOMed. COST Action MP1202 is also acknowledged for supporting visit exchanges. CIBER-BBN is an initiative funded by the VI National R&D&i Plan 2008–2011, Iniciativa Ingenio 2010, Consolider Program, CIBER Actions and financed by the Instituto de Salud Carlos III with assistance from the European Regional Development Fund. C. E. P.-G. acknowledges CAM for a fellowship. We also acknowledge Junta de Extremadura support under Grant GR10149.

6. Supplementary Data. Full experimental section, selected NMR spectra, complete XPS and EPR spectra, UV spectra, toxicity in PBMC and toxicity and inhibition data.

7. References

[1] Y.-C. Yeh, B. Creran, V. M. Rotello, *Nanoscale* **2012**, *4*, 1871-1880.

[2] N. Khlebtsov, L. Dykman, *Chem. Soc. Rev.* **2011**, *40*, 1647–1671.

[3] A. Llevot, D. Astruc, *Chem. Soc. Rev.* **2012**, *41*, 242–257.

[4] S. Krol, R. Macrez, F. Docagne, G. Defer, S. Laurent, M. Rahman, M. J. Hajipour, P. G. Kehoe, M. Mahmoudi, *Chem. Rev.* **2012**, *113*, 1877-1903.

[5] L. Dykman, N. Khlebtsov, *Chem. Soc. Rev.* **2012**, *41*, 2256-2282.

[6] P. M. Tiwari, K. Vig, V. A. Dennis, S. R. Singh, *Nanomaterials* **2011**, *1*, 31-63.

[7] E. C. Dreaden, M. A. Mackey, X. Huang, B. Kanga, M. A. El-Sayed, *Chem. Soc. Rev.* **2011**, *40*, 3391-3404.

[8] H. Gu, P. L. Ho, E. Tong, L. Wang, B. Xu, *Nano Lett.* **2003**, *3*, 1261-1263.

[9] R. W. J. Buckheit, K. M. Watson, K. M. Morrow, A. S. Ham, *Antiviral. Res.* **2010**, *85*, 142–158.

[10] M.-C. Bowman, E. Ballard, C. J. Ackerson, D. L. Feldheim, D. M. Margolis, C. Melander, *J. Am. Chem. Soc.* **2008**, *130*, 6896–6897.

[11] F. Chiodo, M. Marradi, J. Calvo, E. Yuste, S. Penadés, *Beilstein J. Org. Chem.* **2014**, *10*, 1339–1346.

[12] B. Arnáiz, O. Martinez-Ávila, J. M. Falcon-Pérez, S. Penadés, *Bioconjugate Chem.* **2012**, *23*, 814-825.

[13] P. Di Gianvincenzo, M. Marradi, O. M. Martínez-Ávila, L. M. Bedoya, J. Alcamí, S. Penadés, *Bioorg. Med. Chem. Lett.* **2010**, *20*, 2718-2721.

[14] J. Vonnemann, C. Sieben, C. Wolff, K. Ludwig, C. Böttcher, A. Herrmann, R. Haag, *Nanoscale* **2014**, *6*, 2353-2360.

[15] I. A. Scordi-Bello, A. Mosoian, C. J. He, Y. B. Chen, Y. Cheng, G. A. Jarvis, M. J. Keller, K. Hogarty, D. P. Waller, A. T. Profy, B. C. Herold, M. E. Klotman, *Antimicrob. Agents Chemother.* **2005**, *49*, 3607-3615.

[16] J. Balzarini, L. Van Damme, *Lancet* **2007**, *369*, 787-797.

[17] M. Moulard, H. Lortat-Jacob, I. Mondor, G. Roca, R. Wyatt, J. Sodroski, Z. Lu, W. Olson, P. D. Kwong, Q. J. Sattentau, *J. Virol.* **2000**, *74*, 1948-1960.

[18] J. J. Reina, A. Bernardi, M. Clerici, J. Rojo, *Future Med. Chem.* **2010**, *2*, 1141-1159.

[19] L. Chonco, M. Pion, E. Vacas, B. Rasines, M. Maly, M. J. Serramía, L. López-Fernández, F. J. de la Mata, S. Álvarez, R. Gómez, M. A. Muñoz-Fernández, *J. Control. Release* **2012**, *161*, 949-958.

[20] D. Huskens, K. Vermeire, A. T. Profy, D. Schols, *Antiviral Res.* **2009**, *84*, 38–47.

[21] R. G. Denkewalter, J. F. Kolc, W. J. Lukasavage, *US Pat 4, 410, 688* **1983**.

[22] G. R. Newkome, C. N. Moorefield, F. Vögtle, *Dendrimers and Dendrons: Concepts, Syntheses, Applications. Wiley-VCH, Weinheim, Germany.* **2001**.

[23] F. Vögtle, C. A. Schalley, *Top. Curr. Chem.* **2003**, *228*.

[24] D. A. Tomalia, J. M. J. Fréchet, *J. Polym. Sci., Part A: Pol. Chem.* **2002**, *40*, 2719-2728.

[25] J. M. J. Fréchet, D. A. Tomalia, *Dendrimers and Other Dendritic Polymers, Wiley VCH, Weinheim,* **2002**.

[26] D. Astruc, E. Boisselier, C. Ornelas, *Chem. Rev.* **2010**, *110*, 1857–1959.

[27] O. Rolland, C. O. Turrin, A. M. Caminade, J. P. Majoral, *New J. Chem.* **2009**, *33*, 1809-1824.

[28] J. L. Jiménez, M. Pion, F. J. de la Mata, R. Gómez, E. Muñoz, M. Leal, M. A. Muñoz-Fernández, *New J. Chem.* **2012**, *36*, 299-309.

[29] D. Tyssen, S. A. Henderson, A. Johnson, J. Sterjovski, K. Moore, J. La, M. Zanin, S. Sonza, P. Karellas, M. P. Giannis, G. Krippner, S. Wesselingh, T. McCarthy, P. R. Gorry, P. A. Ramsland, R. Cone, J. R. A. Paull, G. R.Lewis, G. Tachedjian, *PLoS ONE* **2010**, *5*, e12309.

[30] Y. H. Jiang, P. Emau, J. S. Cairns, L. Flanary, W. R. Morton, T. D. McCarthy, C. C. Tsai, *AIDS Res. Hum. Retrovir.* **2005**, *21*, 207-213.

[31] E. Arnáiz, E. Vacas-Cordoba, M. Galán, M. Pion, R. Gómez, M. A. Muñoz-Fernández, F. J. de la Mata, *J. Polym. Sci. Part A: Polym. Chem.* **2014**, *52*, 1099–1112.

[32] E. Vacas-Córdoba, M. Galán, R. Gómez, F. J. de la Mata, M. Pion, M. A. Muñoz-Fernández, *Int. J. Nanomed.* **2014**, *9*, 3591-3360.

[33] E. Vacas-Córdoba, E. Arnáiz, M. Relloso, C. Sánchez-Torres, F. García, L. Pérez-Á lvarez, R. Gómez, F. J. de la Mata, M. Pion, M. A. Muñoz-Fernández, *AIDS* **2013**, *27*, 1219–1229.

[34] E. Vacas-Córdoba, E. Arnáiz, R. Gómez, F. J. de la Mata, M. Leal, M. Pion, M. A. Muñoz-Fernández, *AIDS* **2013**, *27*, 2053–2058.

[35] D. Sepúlveda-Crespo, R. Lorente, M. Leal, R. Gómez, F. J. de la Mata, J. L. Jiménez, M. Á. Muñoz-Fernández, *Nanomedicine: NBM* **2014**, *10*, 609–618.

[36] M. Galán, E. Fuentes-Paniagua, R. Gómez, F. J. de la Mata, *Organometallics* **2014**, *33*, 3977−3989.

[37] J. I. Paez, M. Martinelli, V. Brunetti, M. C. Strumia, *Polymers* **2012**, *4*, 355-395.

[38] A. D. Schluter, J. P. Rabe, *Angew. Chem. Int. Ed.* **2000**, *39*, 864-883.

[39] M.-C. Daniel, J. Ruiz, S. Nlate, J. Palumbo, J.-C. Blais, D. Astruc, *Chem. Comm.* **2001**, 2000-2001.

[40] M. K. Kim, Y. M. Jeon, W. S. Jeon, H. J. Kim, S. G. Hong, C. G. Park, K. Kim, *Chem. Commun.* **2001**, 667-668.

[41] G. Jiang, L. Wang, W. Chen, *Mater. Lett.* **2007**, *61*, 278–283.

[42] T. J. Cho, R. A. Zangmeister, R. I. MacCuspie, A. K. Patri, V. A. Hackley, *Chem. Mat.* **2011**, *23*, 2665-2676.

[43] M. C. Daniel, J. Ruiz, D. Astruc, *J. Am. Chem. Soc.* **2003**, *125*, 2617-2628.

[44] J. G. Hardy, C. S. Love, N. P. Gabrielson, D. W. Pack, D. K. Smith, *Org. Biomol. Chem.* **2009**, *7*, 789-793.

[45] T. Takahashi, J. Hirose, C. Kojima, A. Harada, K. Kono, *Bioconjugate Chem.* **2007**, *18*, 1163-1169.

[46] M. Berna, D. Dalzoppo, G. Pasut, M. Manunta, L. Izzo, A. T. Jones, R. Duncan, F. M. Veronese, *Biomacromolecules* **2006**, *7*, 146-153.

[47] J. Pan, M. Wen, D. Yin, B. Jiang, D. He, L. Guo, *Tetrahedron* **2012**, *68*, 2943-2949.

[48] A. M. Caminade, A. Maraval, J. P. Majoral, *Eur. J. Inorg. Chem.* **2006**, 887-901.

[49] S. Yokoyama, A. Otomo, T. Nakahama, Y. Okuno, S. Mashiko, *Top. Curr. Chem.* **2003**, *228*, 205-226.

[50] E. Fuentes-Paniagua, C. E. Peña-González, Marta Galán, R. Gómez, F. J. de la Mata, J. Sánchez-Nieves, *Organometallics* **2013**, *32*, 1789−1796.

[51] C. Fornaguera, S. Grijalvo, M. Galán, E. Fuentes-Paniagua, F. J. de la Mata, R. Gómez, R. Eritja, G. Caldero, C. Solans, *Int. J. Pharm.* **2014**, *478*, 113-123.

[52] Á. Martínez, E. Fuentes-Paniagua, A. Baeza, J. Sánchez-Nieves, R. Gómez, F. J. de la Mata, B. González, M. Vallet-Regí, *Chem. Eur. J.* **2015**, *21*, 15651–15666.

[53] E. Fuentes-Paniagua, M. J. Serramía, J. Sánchez-Nieves, S. Álvarez, M. A. Muñoz-Fernández, R. Gómez, F. J. de la Mata, *Eur. Polym. J.* **2015**, *71*, 61–72.

[54] E. Fuentes-Paniagua, J. Sánchez-Nieves, J. M. Hernández-Ros, J. Soliveri, J. L. Copa-Patiño, R. Gómez, F. J. de la Mata, *Submitted* **2015**.

[55] F. Gonzàlez de Rivera, L.-I. Rodríguez, O. Rossell, M. Seco, N. J. Divins, I. Casanova, J. Llorca, *J. Organomet. Chem.* **2011**, *696*, 2287–2293.

[56] S. García-Gallego, M. Cangiotti, L. Fiorani, A. Fattori, M. Á. Muñoz-Fernández, R. Gómez, M. F. Ottaviani, F. J. de la Mata, *Dalton Trans.* **2013**, *42*, 5874–5889.

[57] M. Galán, J. Sánchez-Rodríguez, M. Cangiotti, S. Garcia-Gallego, J. L. Jimenez, R. Gómez, M. F. Ottaviani, M. A. Muñoz-Fernández, F. J. de la Mata, *Curr. Med. Chem.* **2012**, *19*, 4984-4994.

[58] Y. Pan, S. Neuss, A. Leifert, M. Fischler, F. Wen, U. Simon, G. Schmid, W. Brandau, W. Jahnen-Dechent, *Small* **2007**, *3*, 1941–1949.

[59] C. M. Goodman, C. D. McCusker, T. Yilmaz, V. M. Rotello, *Bioconjugate Chem.* **2004**, *15*, 897.

[60] M. Longmire, P. L. Choyke, H. Kobayashi, *Nanomed. (Lond)* **2008**, *3*, 703–717.

[61] J. Liu, M. Yu, C. Zhou, J. Zheng, *Materials Today* **2013**, *16*, 477-486.

[62] J. G. A. Terlingen, J. Feijen, A. S. Hoffman, *J. Colloid Interface Sci.* **1993**, *155*, 55-65.

[63] M. Volmer, M. Stratmann, H. Viefhaus, *Surf. Interface Anal.* **1990**, *16*, 278-282.

[64] H. Zhongy, X. Liping, H. Sheng, C. Aixi, Q. Jianwei, F. Xisheng, *Plos One* **2013**, *8*, e62050.

[65] N. S. R. Database, http://srdata.nist.gov/xps/.

[66] M. Brust, M. Walker, D. Bethell, D. J. Schiffrin, R. Whyman, *J. Chem. Soc., Chem. Commun.* **1994**, 801-802.

[67] L. Sun, R. M. Crooks, V. Chechik, *Chem. Commun.* **2001**, 359-360.

[68] L. Chen, T. E. Andersson, C. Rissing, S. Yang, S. Chen, D. Y. Son, *J. Mater. Chem. B,* **2013**, *1*, 116-122.

[69] S. García-Gallego, J. S. Rodríguez, J. L. Jiménez, M. Cangiotti, M. F. Ottaviani, M. A. Muñoz-Fernández, R. Gómez, F. J. de la Mata, *Dalton Trans.* **2012**, *41*, 6488-6499.

[70] S. García-Gallego, M. J. Serramía, E. Arnáiz, L. Diaz, M. A. Muñoz-Fernández, P. Gómez-Sal, M. F. Ottaviani, R. Gómez, F. J. de la Mata, *Eur. J. Inorg. Chem.* **2011**, 1657-1665.

[71] D. E. Budil, S. Lee, S. Saxena, J. H. Freed, *J. Magn. Reson. A* **1996**, *120*, 155-189.

[72] E. J. Platt, K. Wehrly, S. E. Kuhmann, B. Chesebro, D. Kabat, *J. Virol.* **1998**, *72*, 2855-2864.

[73] I. García-Merino, N. de las Cuevas, J. L. Jiménez, J. Gallego, C. Gómez, C. Prieto, M. J. Serramía, R. Lorente, M. Á. Muñoz-Fernández, *Retrovirology* **2009**, *6*, 27.

Table of Contents:

Antiviral anionic gold nanoparticles

Water soluble gold nanoparticles (AuNPs) have been isolated with pendant anionic sulfonate carbosilane dendrons. The antiviral properties of dendronized AuNPs are higher than that of free dendrons.

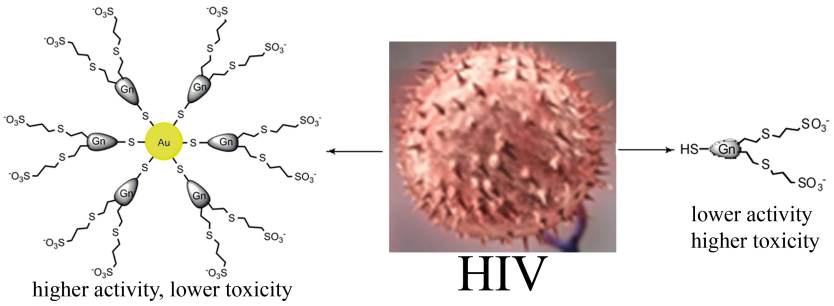

Scheme and figure legends:

Scheme 1. Top: Synthesis of anionic dendrons $HSG_n(SO_3^-)_m$ (n = 1, m = 2 (**4**); n = 2, m = 4 (**5**); n = 3, m = 8 (**6**)). i) $HS(CH_2)_3SO_3^-$, DMPA, hν; ii) HCl. Bottom: Sturctures of dendrons $HSG_n(SO_3^-)_m$ (**4-6**).

Scheme 2. Synthesis of anionic NPs $Au@(SG_n(SO_3^-)_m)$ (n = 1, m = 2 (**7b**); n = 2, m = 4 (**8b**); n = 3, m = 8 (**9b**)). i) $NaBH_4$.

Scheme 3. Synthesis of anionic gold nanoparticles $(Au@(SC12)_x(SG_n(SO_3^-)_m)_y)$ (**7c-9c**) by place-exchange reaction. i) $HSG_n(SO_3^-)_m$ (n = 1, m = 2 (**4**); n = 2, m = 4 (**5**); n = 3, m = 8 (**6**).

Figure 1. **Au@(SG1($SO_3Na)_2$) (7b)**: a) TEM image and, b) Size distribution histogram associated to nanoparticle **7b** functionalized by direct method with sulfonate carbosilane dendrons of first generation (average size = 3.6 nm (20668 measure nanoparticles with Image J program)).

Figure 2. XPS survey spectrum collected for $Au@(SG1(SO_3Na)_2)$ (**7b**), as a representative example of all the samples examined.

Figure 3. High resolution XPS spectra for the S2p region for a) $Au@(SG_1(SO_3Na)_2)$ (**7b**), b) $Au@(SG_2(SO_3Na)_4)$ (**8b**), and c) $Au@(SG_3(SO_3Na)_8)$ (**9b**).

Figure 4. Selected EPR spectra obtained at 150 K for the samples: a) $HSG_1(SO_3^-)_2$ (**4**), b)$HSG_3(SO_3^-)_8$ (**6**), c) $Au@(SG_1(SO_3^-)_2)$ (**7b**), d) $Au@(SG_3(SO_3^-)_8)$ (**9b**).

Figure 5. Relative percentages of the different signals constituting the EPR spectra at 150 K in function of copper(II) concentration for: a) **4**, b) **5**, c) **6**, d) **7a**, e) **7b**, f) **8b**, g) **9b**.

Figure 6. Toxicity of anionic dendrons and NPs. TZM.bl cells were treated in the presence of a range of concentrations from 0.01 μM to 20 μM of dendrons and 0.01 μg/ml to 100 μg/ml of AuNPs for 24 h (A, C) or 48 h (B, D). Dextran 10 μM was used as negative control of cellular death (non toxic compounds)

and DMSO 10% was used as positive control of toxicity. The discontinuous line corresponds to 80% of viability set as limit of toxicity for viable cells. Data represent the mean ± SEM (n=3).

Figure 7. Inhibition of R5-HIV-1_{NLAD8} and X4-HIV-$1_{NL4.3}$ infections in TZM.bl cells by dendrons HSG1$(SO_3Na)_2$ (**4**) and HSG2$(SO_3Na)_4$ (**5**) and NPs Au@(SG1$(SO_3Na)_2$) (**7b**), Au@(SG2$(SO_3Na)_4$) (**8b**), and Au@(SG3$(SO_3Na)_8$) (**9b**). TZM.bl cells were pretreated with increased non-toxic concentrations of dendrons **4** and **5** (A) and NPs **7b-9b** (B), 1 h before HIV-1 infection with R5-HIV-1_{NLAD8} or X4-HIV-$1_{NL4.3}$ isolates at a concentration 50 ng/10^6 cells. TZM.bl cells were lysed and HIV-1 replication was determined at 72 h by quantification of luciferase expression. Antiviral T20 (enfuvirtide, fusion inhibitor) 20µM was used as positive control of the inhibition of HIV-1 infection. The discontinuous line corresponds to 80 % of inhibitory effect on VIH-1 infection. Data represent the mean ± SEM (n=3).

Nanoparticles	**Molar Ratio Au/S**		**D (nm)[a]**	**Molecular formula[b]**	**Av. MW ($gmol^{-1}$)[b]**	**N[c]**	**ZP (mV)**
	Theoretic	Obtained					
$Au@(SG_1(SO_3Na)_2)$ **(7a)**	1:1	3.04:1	2.4	$Au_{427}(C_{15}H_{31}Na_2O_6S_5Si)_{140}$	159953	280	-22.8
$Au@(SG_1(SO_3Na)_2)$ **(7b)**	2:1	5.65:1	3.6	$Au_{1441}(C_{15}H_{31}Na_2O_6S_5Si)_{255}$	421978	510	-31.4
$Au@(SG_2(SO_3Na)_4)$ **(8b)**	4:1	10.01:1	3.4	$Au_{1214}(C_{33}H_{69}Na_4O_{12}S_9Si_3)_{121}$	374956	484	-29.1
$Au@(SG_3(SO_3Na)_8)$ **(9b)**	8:1	20.16:1	3.0	$Au_{834}(C_{69}H_{145}Na_8O_{24}S_{17}Si_7)_{41}$	257929	328	-40.1
$Au@(SG_1(SO_3Na)_2)(SC12)$ **(7c)**			1.2				-57.0
$Au@(SG_2(SO_3Na)_4)(SC12)$ **(8c)**			1.8				-30.1
$Au@(SG_3(SO_3Na)_8)(SC12)$ **(9c)**			1.0				-63.9

Table 1. Selected data of AuNP **7-9**. a) Obtained by TEM; b) Obtained by TGA and elemental analysis; c) Number of sulfonate groups by NP.

Spectral Component	g_{xx}	g_{yy}	g_{zz}	A_{xx} (G)	A_{yy} (G)	A_{zz} (G)	LW (G)
Signal 0	2.017	2.096	2.328	-8	-8	160	40
Signal 1	2.065	2.095	2.398	-8	-8	125	30
Signal 2	2.079	2.154	2.322[#]	-5	-20	116[#]	70

[#]very low accuracy, due to the poor resolution of this signal in the parallel region of gii and Aii

Table 2. Magnetic parameters used for computations of the signals constituting the spectra of copper(II) complexed by dendron **6**.

Text for the Table of Contents

Antiviral anionic gold nanoparticles

Water soluble gold nanoparticles (AuNPs) have been isolated with pendant anionic sulfonate carbosilane dendrons. The antiviral properties of dendronized AuNPs are higher than that of free dendrons.

Keywords: gold nanoparticles, sulfonate carbosilane dendrons, antivirus agents, HIV, EPR.